Experimental Observation of Classical Dynamical Monodromy

M. P. Nerem, D. Salmon, S. Aubin, and J. B. Delos
Department of Physics, College of William and Mary, 300 Ukrop Way, Williamsburg, Virginia 23185-8795, USA

(Received 6 November 2017; published 30 March 2018)

A Hamiltonian system is said to have nontrivial monodromy if its fundamental action-angle loops do not return to their initial topological state at the end of a closed circuit in angular momentum-energy space. This process has been predicted to have consequences which can be seen in dynamical systems, called *dynamical monodromy*. Using an apparatus consisting of a spherical pendulum subject to magnetic potentials and torques, we observe nontrivial monodromy by the associated topological change in the evolution of a loop of trajectories.

DOI: 10.1103/PhysRevLett.120.134301

Introduction.—Classical mechanics is an old subject in which new physics seldom appears. However, a body of recent work is developing on phenomena collectively called *Hamiltonian monodromy*. In its "static" manifestation, action variables are multivalued functions of conserved quantities. This leads to dynamical consequences, where a loop or cloud of particles can be made to evolve smoothly into a topologically different loop. Monodromy was first introduced theoretically [1] as a change in the topology of action-angle coordinates in the "champagne bottle" system. Since then, it has been shown to exist in several physical systems, including the symmetric top and spherical pendulum [2], a top in a fluid [3], and a resonant swing spring [4].

This classical phenomenon was extended to quantum mechanics [5]. Because action variables are multivalued, their corresponding quantum numbers are multivalued, so there is no unique assignment of quantum numbers to quantum states. The archetypal manifestation of monodromy on the global structure of a quantum system is a spatial defect in the lattice of allowed eigenvalues [6].

This quantum manifestation of monodromy has been predicted theoretically in the energy spectra of atomic hydrogen [7], ellipsoidal billiards [8], H_2^+ and HHe^{2+} [9], H_2O and quasilinear molecules [10], dipolar molecules in electric fields [11], the quantum swing spring [12], which is a model for the CO_2 molecule [13], and trapped Bose gases [14]. Related phenomena have also been characterized [15], such as fractional monodromy [16], bidromy [17], and the combination thereof, predicted in HOCl [18]. Monodromy also shows up in collective vibrations of nucleons in bound nuclei (interacting boson model) [19], attractors in theories of nonlinear waves [20] and, most recently, Dicke superradiance [21].

The above are called static manifestations of monodromy; they arise from smooth connections of action-angle coordinates on families of static phase-space tori that are present in integrable classical systems. "Dynamical" manifestations of monodromy are analogous topological changes in loops of particles that occur as a system evolves in time [22]. We apply a time dependent perturbation to a loop of particles in a system with monodromy, and follow the loop as it evolves into a topologically different loop. This change is classical dynamical monodromy.

While quantum static monodromy has been demonstrated in the spectra of some molecular systems [23], we know of only one measurement on a classical system that displayed static manifestations of monodromy [24]. We report here the first experimental demonstration of dynamical monodromy. Our experimental design is an adaptation of the prototypical monodromy system: particles moving in a champagne bottle potential. The dynamical consequences of monodromy in this system have been discussed theoretically [22] and are summarized in the following section.

Dynamical monodromy.—Consider particles of unit mass restricted to a 2D plane, in a cylindrically symmetric potential with a central barrier, $V(\rho)$:

$$V(\rho) = -a\rho^2 + b\rho^4 \quad (a, b > 0), \tag{1}$$

$$H(\boldsymbol{q},\boldsymbol{p}) = \frac{1}{2}(p_x^2 + p_y^2) + V(\rho) = h, \tag{2}$$

$$L(\boldsymbol{q},\boldsymbol{p}) = xp_y - yp_x = \ell. \tag{3}$$

The Hamiltonian and angular momentum are conserved quantities, with their values denoted (ℓ, h). The space of values (ℓ, h) is called angular momentum-energy space, but we prefer a name that connects with quantum mechanics, spectrum space. A *level set* of these functions is the set of phase-space points having fixed values of angular momentum and energy, $\{\boldsymbol{z} = (x, y, p_x, p_y) | L(\boldsymbol{z}) = \ell, H(\boldsymbol{z}) = h\}$. By the Liouville-Arnold theorem [25], these level sets, defined by the angular momentum and energy values, are topologically equivalent to tori (with the exception of one

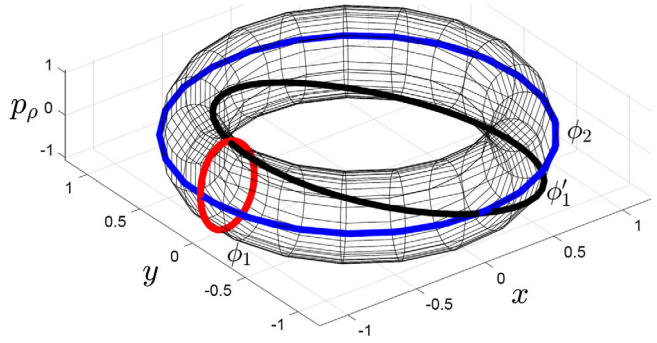

FIG. 1. Angle loops ϕ_1 (red line) and ϕ_2 (blue line) are plotted on a torus. After going around a monodromy circuit, ϕ_1 smoothly changes into $\phi_1' = \phi_1 + \phi_2$ (black line).

set). To visualize the torus we can express any canonical momentum, here we choose p_ρ, as a function of configuration coordinates and a given value of angular momentum and energy,

$$p_\rho(\boldsymbol{q}; \ell, h) = \left\{ 2\left(h - \frac{\ell^2}{2\rho^2} - V(\rho) \right) \right\}^{1/2}. \qquad (4)$$

Figure 1 is the corresponding torus for $\ell = 1$, $h = -1$, $a = 5$, and $b = 3$.

The level set corresponding to ($\ell = 0$, $h = 0$) is the one set that is not a torus. The derivatives of $H(\boldsymbol{z})$ and $L(\boldsymbol{z})$ vanish at $\boldsymbol{z} = \boldsymbol{0}$, making their phase space gradients linearly dependent at that point. The spectrum space point, ($\ell = 0$, $h = 0$), is a singular value, called the *monodromy point*, and the corresponding level set is called a pinched torus [26]. Action-angle variables are not defined on this level set, and the remaining set of nonsingular values in spectrum space is not simply connected. A consequence is that the canonical action-angle variables can, and in fact do, become multivalued functions of (ℓ, h). A monodromy circuit is defined as *any* closed circuit in spectrum space surrounding the monodromy point. When we examine the changes of action-angle loops on the circuit, the initial and final tori are the same, but, as shown in Fig. 1, one of the canonical angle variables has smoothly changed into a different fundamental loop. This is a static manifestation of monodromy.

In dynamical monodromy, this same topological change can be implemented by driving a loop of noninteracting particles around a monodromy circuit. First we start with a family of noninteracting particles on the initial torus ($\ell = 0$, $h < 0$) with initial positions and momenta corresponding to the ϕ_1 canonical angle loop of Fig. 1. In position space, particles oscillate radially between the inner and outer classically forbidden regions as shown in Fig. 2 I. Then we apply external forces to dynamically change the particles' angular momenta and energies, following a monodromy circuit in spectrum space, $(\ell(t), h(t))$, around the monodromy point.

Several steps are required to drive the particles around this circuit. (i) Start all particles with the same energy $h_0 < 0$ and angular momentum $\ell = 0$ as shown in Fig. 2 I. (ii) Apply external forces so the particles are given positive angular-momentum and begin to rotate around the classically forbidden region, shown in Fig. 2 II. (iii) Increase the energy of each particle to $h > 0$, shown in Fig. 2 III. (iv) Reduce the angular momentum to zero (when we focus on the structure of the loop in configuration space, this is the critical point on the monodromy circuit). (v) Continue to reduce the angular momentum to a negative value. During this evolution (steps iii–v), the angular momentum is zero for an instant and the classically forbidden region vanishes simultaneously, shown in Fig. 2 IV. After this critical moment the classically forbidden region reappears *inside* the loop and we see the predicted topological change, shown in Fig. 2 V. The family of particles had been confined to one side of the classically forbidden region, but now the family surrounds the forbidden region. The remainder of the monodromy circuit returns the angular momentum and energy to their initial values. (vi) Reduce the energy of each particle to $h < 0$ as seen in Fig. 2 VI. (vii) Apply final torques to bring the angular momentum back to zero and the energy to the initial value h_0. Under "ideal" evolution, all particles have equal angular momenta and energies at all times, and the final values are equal to the initial values. However, this is not required to observe the change in topology of the loop of particles, as seen in Figs. 2 I and VIII.

Computation [22] has shown that the loop of particles follows the behavior of the angle loop: at the end of the circuit, the loop will have changed its topological structure. This topological change is the very definition of dynamical monodromy. The loop of particles, as it evolves in time, has experienced the same topological change as the angle loops in Fig. 1. Here we carry out this process in the laboratory [27].

The apparatus.—To realize this evolution in a classical experiment, we can observe a family of trajectories of a single object with different initial conditions instead of several noninteracting particles. We constructed a spherical pendulum using a rigid Al rod (length $d = 2.502 \pm 3.2 \times 10^{-3}$ m) with a permanent magnet at its end. The kinetic energy for our spherical pendulum is $\mathrm{KE} = \frac{1}{2} I_{\mathrm{pend}} (\sin^2\theta \dot{\phi}^2 + \dot{\theta}^2)$. The rigid pendulum and magnet together have a moment of inertia I_{pend}. The magnet [28] is a cylinder neodymium magnet of mass 382 ± 0.1 g and magnetic moment of 56.8 ± 0.7 J/T. It was modeled as a dipole moment $|\mu|$ aligned coaxially with the pendulum. A circular coil placed beneath the center of the pendulum provides a cylindrically symmetric repulsive force on the magnet creating the inner barrier of the potential. Thus the full potential energy is

$$V_{\mathrm{well}} = (m_d d_{cm} + m d) g \cos\theta - \boldsymbol{\mu} \cdot \boldsymbol{B}_{\mathrm{coil}}, \qquad (5)$$

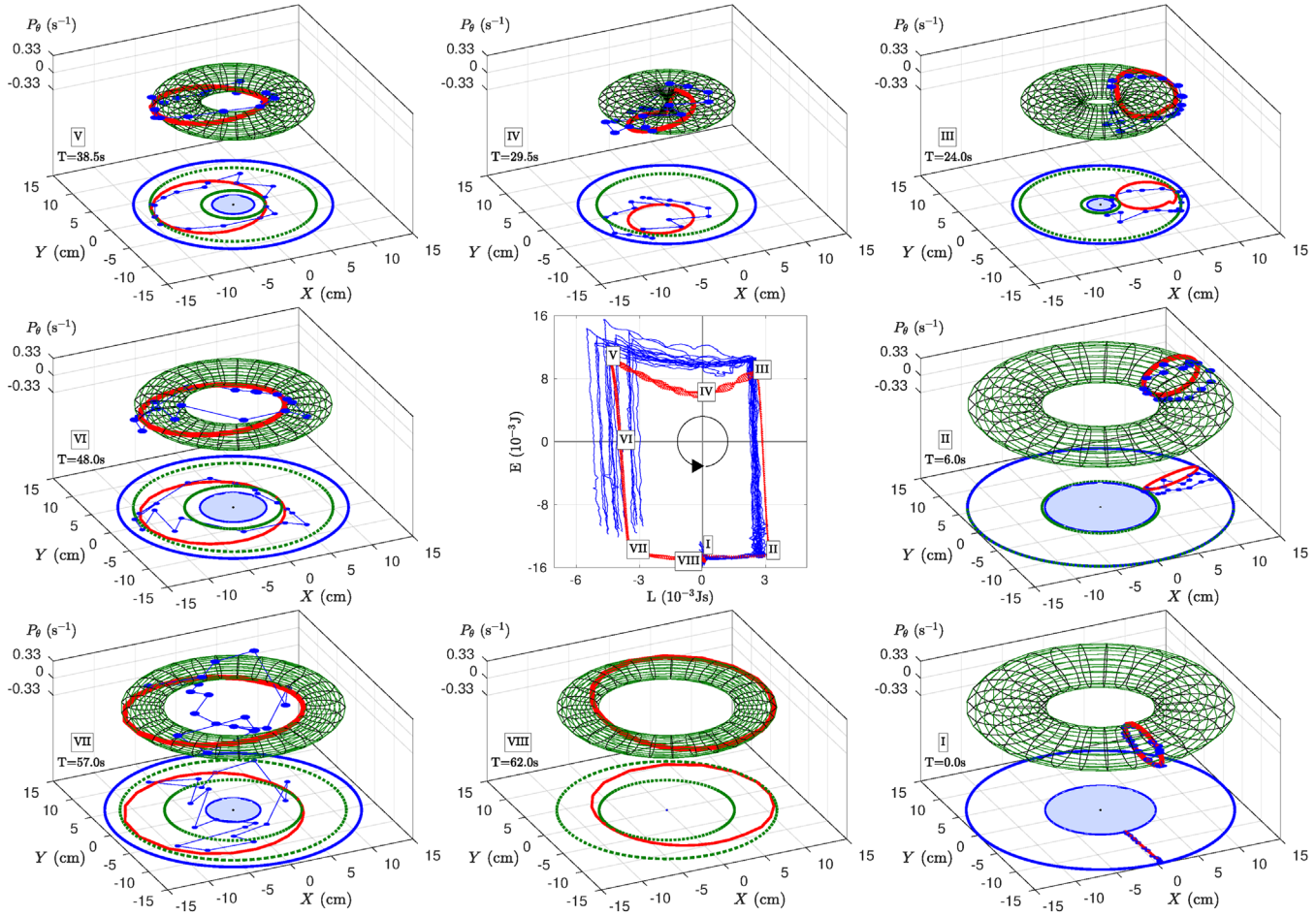

FIG. 2. A dynamical monodromy loop with theory (red lines) and experiment (blue lines). The center plot shows the monodromy circuit in spectrum space while the outer plots are snapshots of the torus and loop of particles at marked points along the circuit. The tori are generated using P_θ, defined in Eq. (6). The filled blue sections in XY space are the inner turning radii for the experimental data and the green dashed circles are projections of the inner and outer radii of the tori. The loop of particles undergoes a topological change (see III and V) as the classically forbidden region disappears in the intervening time, IV. I and VIII correspond to the same torus defined by ($\ell = 0$, $h < 0$). By this time, however, the experiment has diverged from the ideal path and does not complete the circuit.

where m_d is the mass of the rod (713 ± 1 g), m the mass of the magnet, d_{cm} the center of mass of the pendulum, and $\boldsymbol{B}_{\text{coil}}$ the magnetic fields from the center coil [29]. The tori seen in Fig. 2 were plotted using the P_θ momentum cast as a function of the energy and angular momentum,

$$P_\theta = \left\{ 2I_{\text{pend}} \left(h - \frac{\ell^2}{2I_{\text{pend}} \sin^2\theta} \right) \right\}^{1/2}. \tag{6}$$

The current in the center coil defines the height of the inner barrier. Instead of adjusting the energy of the pendulum, we can decrease the current (and the resulting field strength of the central coil), lowering the barrier.

A camera recording at 30 frames per second mounted above the system tracks the pendulum's position. We use Savitzki-Golay (SG) convolution [30] to smooth the position data. Similarly, the velocity was found with a five point first order SG convolution. Subsequent quantities, such as the energy and angular momentum, were calculated using the SG-smoothed position and velocity. The experiment used 18 "particles" (i.e. initial conditions) on the initial angle loop. In Fig. 2, we connect initially adjacent particles to visualize the loop in configuration and phase space.

To control the angular momentum, four square coils surround the perimeter of the pendulum and are connected in two Helmholtz pairs. Partially inspired by the design of time-orbiting-potential (TOP) traps for cold atoms [31], this configuration is shown in Fig. 3. Expressions for the fields generated by these coils are taken from [32]. The forces from these coils on the pendulum can sum in any direction in the xy plane (any force along the length of the pendulum is negated by its rigidity). By adjusting the currents in these coil pairs, we create and maintain a net azimuthal force on the magnet, thereby controlling the angular momentum of the pendulum. The timing of changes of current in these coils is set by the precession frequency of the pendulum for

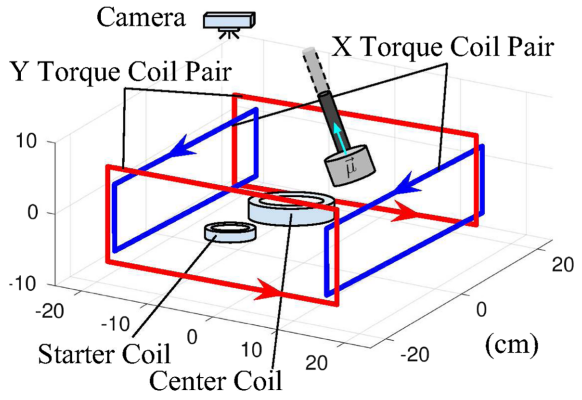

FIG. 3. Diagram of our apparatus. Shown (to scale) are the starter coil, central barrier coil and torque coils. The magnet, camera position, and pendulum are also shown (not to scale), though the pendulum extends beyond the top of the figure.

each particular initial condition, as determined by *a priori* simulation, as seen in Fig. 4. This simulation is a numerical integration of our model Hamiltonian, given the initial conditions obtained via the camera. We do not have any active feedback system to adjust the forces to the instantaneous location of the pendulum. Lastly, there is a small coil off-center, beneath the pendulum, which is used to capture and release the pendulum from a consistent location. All of the electronics are managed via an Arduino microcontroller [33].

A difficult aspect of this experiment is that, because the potential energy, Eq. (5), is cylindrically symmetric, the angular motion of the pendulum is at best neutrally stable. There are instabilities in the pendulum's motion caused by asymmetries in the center coil. Further exacerbating the stability is the timing of external "torquing" forces, as they are dependent on the predicted position at any given time. Any deviation between the pendulum's actual and simulated position will grow due to a nonideal torque being applied. Hence the pendulum easily drifts away from the location computed in the simulation, and torque forces can destabilize the angular motion. For these reasons we record multiple trials [34] for each particle. When we plot the positions of the particles, we use the "trimmed mean," the mean position of the middle 50% of the experimental runs.

Figure 2V compares the experimental data with simulation right after the monodromy circuit has crossed the critical point ($\ell = 0,\ h > 0$). The loop of particles has changed from being on one side of the classically forbidden region to surrounding it instead. Comparing with the simulation of the monodromy circuit in Fig. 2 we see that our experiment has followed a slightly different monodromy circuit. As a result of the spread in spectrum space and especially the angular drift of particles from their simulated positions, the family was unable to complete the monodromy circuit by returning to $\ell = 0$. Nevertheless, the topological change is robust and visible in Figs. 2IV–VII.

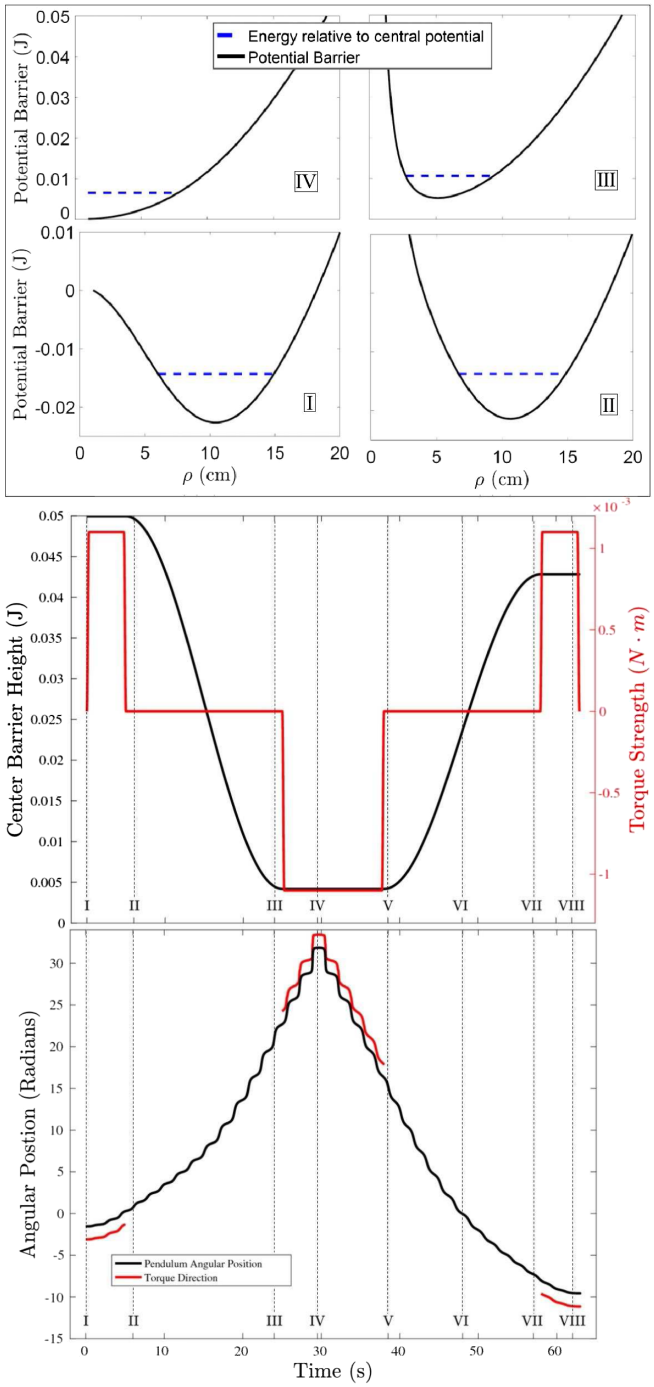

FIG. 4. Top: our potential, $V(\rho) + \ell^2/(2m\rho^2)$, at the first four time steps. Zero energy is in reference to the coil potential energy at $\rho = 0$. Middle: timing sequence of our experiment, showing the barrier height and magnitude of torques on each particle. The difference in initial and final barrier heights is a characterization of the energy lost due to friction over the course of the experiment. Bottom: representative timing sequence of the torque coils tailored *a priori* to keep an azimuthal applied force for a particular trajectory (this figure is shown for the particle that begins on the outer turning radius).

Conclusion.—We have constructed a spherical pendulum apparatus to display the topological change associated with dynamical Hamiltonian monodromy. The change occurs on a family of particles with initial conditions corresponding to a canonical angle loop in phase space. The topological change is robust and both theory and experiment show it, even though the evolution of the pendulum towards the end of the circuit is unstable. This experimental observation makes tangible a phenomenon described in abstract action-angle variables on tori in phase space. Here the topological changes are readily observable on particles in configuration space. Now that dynamical monodromy has been observed in perhaps its simplest system, the way may become clearer for dynamical manifestations to be observed in the multitude of physical systems with Hamiltonian monodromy. An experimental design for cold atomic gases has already been published [22].

Like static monodromy, dynamical monodromy also has a quantum analog, which will be shown in a separate paper. A wave packet state evolving under forces displays the same topological change that is shown here [35].

We thank Dr. W. Cooke and Dr. N. Zobin for their many helpful discussions, Dr. C. Chen for providing Supplemental Figs. 2 and 3, and Dr. D. Manos for his enthusiastic support. This work was financially supported by the College of William and Mary and by NSF Grant No. 1404372.

D. S. and M. P. N. contributed equally to this Letter.

[1] J. J. Duistermaat, Commun. Pure Appl. Math. **33**, 687 (1980).
[2] R. Cushman and L. Bates, *Global Aspects of Classical Integrable Systems* (Springer, New York, 1997).
[3] L. Bates and M. Zou, Nonlinearity **6**, 313 (1993).
[4] H. Dullin, A. Giacobbe, and R. Cushman, Physica D (Amsterdam) **190**, 15 (2004).
[5] R. Cushman and J. J. Duistermaat, Bull. Am. Math. Soc. **19**, 475 (1988).
[6] See Supplemental Material at http://link.aps.org/supplemental/10.1103/PhysRevLett.120.134301 for supplemental Fig. 1.
[7] R. Cushman and D. Sadovski, Physica D (Amsterdam) **142**, 166 (2000); C. Schleif and J. B. Delos, Phys. Rev. A **76**, 013404 (2007); **77**, 043422 (2008); K. Efstathiou, O. V. Lukina, and D. A. Sadovskií, Phys. Rev. Lett. **101**, 253003 (2008); K. Efstathiou and D. A. Sadovskií, Rev. Mod. Phys. **82**, 2099 (2010).
[8] H. Waalkens and H. R. Dullin, Ann. Phys. (Amsterdam) **295**, 81 (2002).
[9] H. Waalkens, H. R. Dullin, and P. H. Richter, Physica D (Amsterdam) **196**, 265 (2004).
[10] M. S. Child, T. Weston, and J. Tennyson, Mol. Phys. **96**, 371 (1999).
[11] I. N. Kozin and R. M. Roberts, J. Chem. Phys. **118**, 10523 (2003); C. A. Arango, W. W. Kennerly, and G. S. Ezra, Chem. Phys. Lett. **392**, 486 (2004).
[12] A. Giacobbe, R. H. Cushman, D. A. Sadovski, and B. I. Zhilinski, J. Math. Phys. (N.Y.) **45**, 5076 (2004).
[13] R. H. Cushman, H. R. Dullin, A. Giacobbe, D. D. Holm, M. Joyeux, P. Lynch, D. A. Sadovskií, and B. I. Zhilinskií, Phys. Rev. Lett. **93**, 024302 (2004).
[14] H. Waalkens, Europhys. Lett. **58**, 162 (2002).
[15] "Berry phase jumps" found in graphene also have some similarities to Hamiltonian monodromy. See J. F. Rodriguez-Nieva and L. S. Levitov, Phys. Rev. B **94**, 235406 (2016).
[16] N. N. Nekhoroshev, D. A. Sadovski, and B. I. Zhilinskii, Comp. Rend. Math. **335**, 985 (2002); Ann. Inst. Henri Poincaré **7**, 1099 (2006).
[17] K. Efstathiou and D. Sugny, J. Phys. A **43**, 085216 (2010); D. Sadovski and B. Zhilinski, Ann. Phys. (Amsterdam) **322**, 164 (2007).
[18] E. Assémat, K. Efstathiou, M. Joyeux, and D. Sugny, Phys. Rev. Lett. **104**, 113002 (2010).
[19] P. Cejnar, M. Macek, S. Heinze, J. Jolie, and J. Dobe, J. Phys. A **39**, L515 (2006).
[20] D. Sugny, A. Picozzi, S. Lagrange, and H. R. Jauslin, Phys. Rev. Lett. **103**, 034102 (2009).
[21] M. Kloc, P. Strnsk, and P. Cejnar, J. Phys. A **50**, 315205 (2017).
[22] J. B. Delos, C. R. Schleif, and G. Dhont, J. Phys. Conf. Ser. **99**, 012005 (2008); J. Delos, G. Dhont, D. A. Sadovski, and B. I. Zhilinski, Europhys. Lett. **83**, 24003 (2008); C. Chen, M. Ivory, S. Aubin, and J. B. Delos, Phys. Rev. E **89**, 012919 (2014).
[23] M. Winnewisser, B. P. Winnewisser, I. R. Medvedev, F. C. D. Lucia, S. C. Ross, and L. M. Bates, J. Mol. Struct. **798**, 1 (2006).
[24] N. J. Fitch, C. A. Weidner, L. P. Parazzoli, H. R. Dullin, and H. J. Lewandowski, Phys. Rev. Lett. **103**, 034301 (2009).
[25] V. Arnol'd, *Geometrical Methods in the Theory of Ordinary Differential Equations* (Springer, New York, 1988).
[26] See Supplemental Material at http://link.aps.org/supplemental/10.1103/PhysRevLett.120.134301 for supplemental Fig. 2.
[27] See Supplemental Material at http://link.aps.org/supplemental/10.1103/PhysRevLett.120.134301 for a video of this experiment.
[28] Specifically, the magnet is a K&J Magnetics RY04X0.
[29] T. Bergeman, G. Erez, and H. J. Metcalf, Phys. Rev. A **35**, 1535 (1987).
[30] A. Savitzky and M. J. E. Golay, Anal. Chem. **36**, 1627 (1964).
[31] V. G. Minogin, J. A. Richmond, and G. I. Opat, Phys. Rev. A **58**, 3138 (1998).
[32] M. Misakian, J. Res. Natl. Inst. Stand. Technol. **105**, 557 (2000).
[33] The model used was an Arduino Due A000062.
[34] For a given initial condition, i.e. "particle," we record either five or ten trials.
[35] C. Chen and J. B. Delos (to be published); See Supplemental Material at http://link.aps.org/supplemental/10.1103/PhysRevLett.120.134301 for supplemental Fig. 3.